

Joining of Aluminum Alloy 5052 and Low-Carbon Steel by Laser Roll Welding

A combination of laser heating and roll welding is suggested to join aluminum Alloy 5052 and low-carbon steel sheets

BY M. J. RATHOD and M. KUTSUNA

ABSTRACT. Low-carbon steel and aluminum Alloy 5052 sheets were diffusion welded using different conditions of time, temperature, and pressure in order to understand the kinetics of diffusion and the microstructure of the interface layer. High pressures accelerated intermetallic compound formation at the interface. The interface layer consisted of aluminum-rich brittle intermetallic compounds (FeAl_3 and Fe_2Al_5), which made the joints brittle.

In laser roll welding, steel and aluminum sheets in a lap-joint configuration are subjected to laser heating and immediate rolling for intimate contact. Laser heating provides high temperature in a short time for melting of the aluminum alloy and diffusion. It results in formation of a thin interface layer. When the temperature is above 1473 K (1200°C), formation of iron-rich (Fe-rich) intermetallic compounds (FeAl and Fe_3Al) is encouraged. Travel speed and roll pressure were varied and resultant joints were characterized by optical microscopy, electron-probe microanalysis (EPMA), scanning electron microscopy (SEM), X-ray diffraction, and tensile shear testing. The laser roll welded interface layer contains brittle aluminum-rich (Al-rich) intermetallic compounds on the aluminum side and slightly ductile Fe-rich intermetallic compounds on the steel side. As the travel speed increases, thinner interface layers are formed and the percentage of Fe-rich intermetallic compounds in them increases. This increases the shear strength of the joints from 11.0 to 55.9 MPa. Interface layers with a thickness of 4 to 5 μm , containing 25 to 40% Fe-rich intermetallic compounds, gave maximum shear strength.

Introduction

Hybrid structures of aluminum alloy and steel are suggested for reducing the weight of automobiles to improve fuel ef-

M. J. RATHOD and M. KUTSUNA are with Department of Material Processing Engineering, School of Engineering, Nagoya University, Nagoya, Japan.

iciency and control air pollution (Refs. 1, 2). Therefore, joining steel and aluminum alloy in different shapes is receiving attention. However, iron and aluminum are not compatible metals as far as fusion welding is concerned. The reason for this is attributed to the large difference between their melting points (933 K for Al and 1811 K for Fe), the nearly zero solid solubility of iron in aluminum, and the formation of brittle intermetallic compounds such as Fe_2Al_5 and FeAl_3 . Further, differences in their thermal properties — like expansion coefficients, conductivities, and specific heats — lead to internal stresses after fusion welding. Therefore, fusion welds of iron and aluminum suffer from heavy cracking with brittle failure in service.

The Fe-Al phase diagram is shown in Fig. 1 (Ref. 3). The intermetallic compounds present on it are grouped as Fe-rich compounds (FeAl and Fe_3Al) and Al-rich compounds (FeAl_2 , Fe_2Al_5 , and FeAl_3). Table 1 summarizes their composition and crystal structures (Refs. 3, 4). In addition to these stable compounds, metastable compounds (FeAl_6 , Fe_2Al_9 , and FeAl_x) are also shown in Table 1 (Ref. 5). Mechanical properties like hardness, fracture toughness K_{IC} values by indentation fracture method, compressive strength, and strain under compression of cast intermetallic compounds are shown in Table 2 (Ref. 6). While Al-rich intermetallic compounds are hard and brittle (0% compressive strain), Fe-rich intermetallic compounds show slight ductility (0.45 and 0.8% compressive strain). Iron-rich intermetallic compounds also possess higher compressive strength than Al-rich intermetallic compounds.

Diffusion Welding

The effect of temperature on diffusion coefficients is shown in Fig. 2 (Ref. 7). Diffusion of iron into aluminum is much faster than vice versa. The condition is favorable for forming brittle Al-rich intermetallic compounds in the interface layer because iron atoms are fewer in number after migrating into the aluminum side. As Al-rich intermetallic compounds are brittle, diffusion-welded joints show poor strength unless insert material is used to control their formation (Refs. 8, 9).

Kinetics of Intermetallic Compound Formation

When a dissimilar metal combination involves formation of intermetallic compound at the interface, it takes place in two stages. Initially, supersaturated solid solution is formed due to migration of atoms across the interface. When composition of supersaturated solid solution reaches to a sufficient level, it transforms into an intermetallic compound (Ref. 10). Therefore, the time before the intermetallic compound appears at the interface is called “incubation time” during which supersaturated solid solution is enriched by diffusing atoms. Activation energy for the formation of supersaturated solid solution during the incubation time is denoted as E_{Sol} . Effective activation energy for the subsequent transformation of supersaturated solid solution into intermetallic compound is denoted as E_{Eff} . The total activation energy for the formation of intermetallic compound (E_{IMC}) can be defined as

$$E_{IMC} = E_{Sol} + E_{Eff} \quad (1)$$

This means that E_{IMC} is greater than E_{Sol} .

When there is a large difference in diffusion rates (as in the case of Fe-Al), the solute atoms and solvent lattice will be decided and the formation of supersaturated solid solution will be favored on one side of the interface. The rate of formation of supersaturated solid solution (\dot{N}_{Sol}) within the incubation time will simply depend on the diffusion of solute atoms in the solvent lattice. The Arrhenius equation for the

KEY WORDS

Dissimilar Metals
Diffusion Welding
Kirkendall Porosity
Laser Roll Welding
Lap Joint
Intermetallic Compound

formation of supersaturated solid solution will be

$$\tilde{N}_{Sol} = k_{Sol} \exp[-E_{Sol}/RT] \quad (2)$$

where k_{Sol} is rate constant in incubation time prior to intermetallic compound formation, R is gas constant, and temperature of diffusion is T in K.

Similarly, rate of transforming the supersaturated solid solution into intermetallic compound (\tilde{N}_{Eff}) is given by

$$\tilde{N}_{Eff} = k_{Eff} \exp [-E_{Eff}/RT] \quad (3)$$

where, k_{Eff} is rate constant for converting supersaturated solid solution into intermetallic compound. Effective activation energy, E_{Eff} depends on the factors involved in this transformation.

$$E_{Eff} = nW + E_{cr} + ne \quad (4)$$

where nW is the activation energy essential for localized fluctuations in composition, E_{cr} is the activation energy involved in restructuring of the crystal lattice when the intermetallic phase is formed, and ne is the deformation energy of the matrix surrounding the nucleus.

Because of the difference in factors involved in formation of supersaturated solid solution (involving atomic diffusion) and transformation of supersaturated solid solution into intermetallic compound (Equation 4), the rate constants k_{Sol} and k_{Eff} are different.

The value of activation energy for the formation of supersaturated solid solution (E_{Sol}) will always remain constant (in case of Al diffusing in Fe, it is 135 kJ/mol). Once the transformation of supersaturated solid solution into intermetallic compound starts, its rate will vary depending on the diffusion of solute atoms into the intermetallic compound layer formed. In this way, in addition to the previously stated factors (Equation 4), another factor (diffusion coefficient for diffusion of solute atoms in intermetallic compound) will come into the picture. A further complex situation will arise when multiple layers of different intermetallic compounds are formed. The latter situations were not considered in this work.

When aluminum is to be diffusion welded, E_{Eff} is further increased due to the hindrance caused by aluminum oxide film present on its surface. The film is tenacious, stoichiometric, and highly stable in nature.

In general, during diffusion welding, intimate contact at the interface is important; a small contact area leads to a poor joint. Pressure during diffusion welding helps in deformation of contacting asperities at the interface by causing yielding and

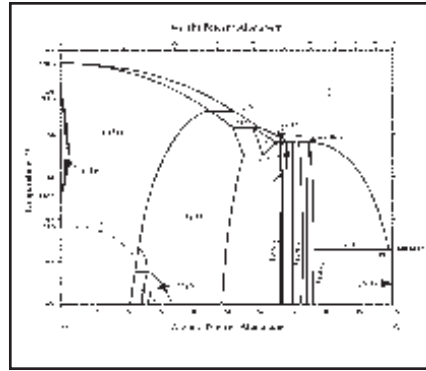


Fig. 1 — Fe-Al equilibrium diagram.

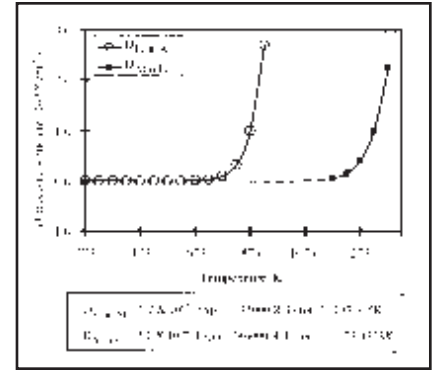


Fig. 2 — Effect of temperature on diffusion coefficients for iron and aluminum.

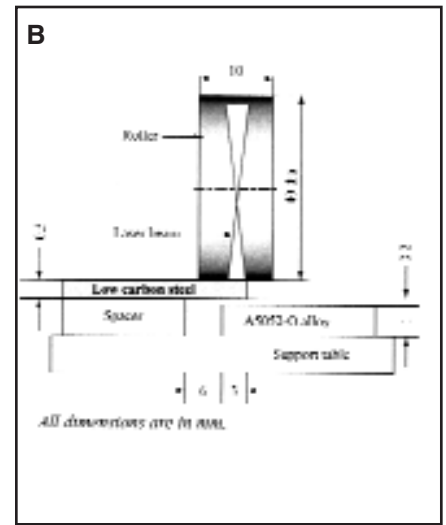
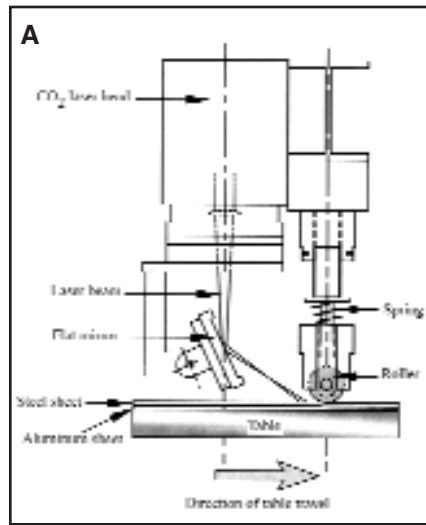


Fig. 3 — A — Schematic diagram of laser roll welding process; B — details of sheet clamping with lap joint configuration.

Table 1 — Composition and Crystal Structures of Intermetallic Compounds of Fe-Al

Type of Intermetallic Compound	Wt-% of Fe	Pearson Symbol	Crystal Structure
Fe ₃ Al	86.06	cF16	FCC
FeAl	67.31	cP8	Cubic
FeAl ₂	50.72	aP18	Triclinic-anorthic
Fe ₂ Al ₅	45.16	mP22	Monoclinic
FeAl ₃	40.70	mC102	BC monoclinic
FeAl ₆ metastable	25.55	oC28	Orthorhombic
Fe ₂ Al ₉ metastable	31.39	mP22, D8 _d	Monoclinic
FeAl _x metastable	Unknown	Unknown	Unknown

Table 2 — Mechanical Properties of Cast Fe-Al Intermetallic Compounds

Type of Intermetallic Compound	Vickers Hardness (9.8 N)	Fracture Toughness K _{IC} , MPa·m ^{1/2}	Compressive Strength, MPa	Compressive Strain, %
FeAl ₃	892	2.15	200	0.00
Fe ₂ Al ₅	1013	2.30	240	0.00
FeAl ₂	Unknown	Unknown	Unknown	Unknown
FeAl	470	Unknown	670	0.45
Fe ₃ Al	330	Unknown	560	0.80

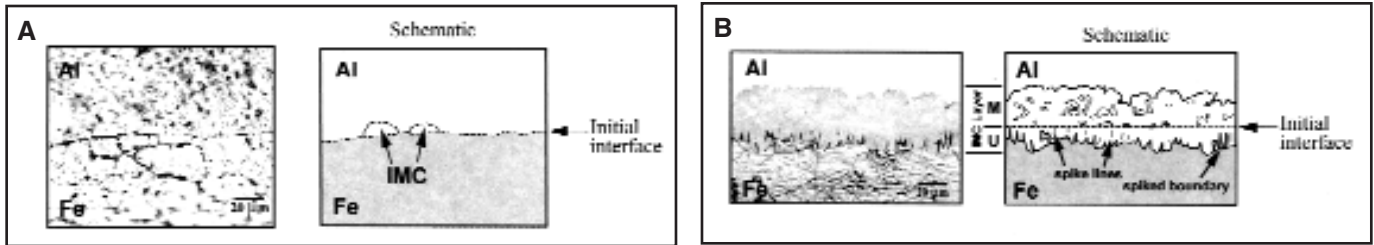


Fig. 4 — Effect of holding temperature on the interface microstructures of diffusion welded specimens. A — Holding temperature 823 K; B — holding temperature 873 K.

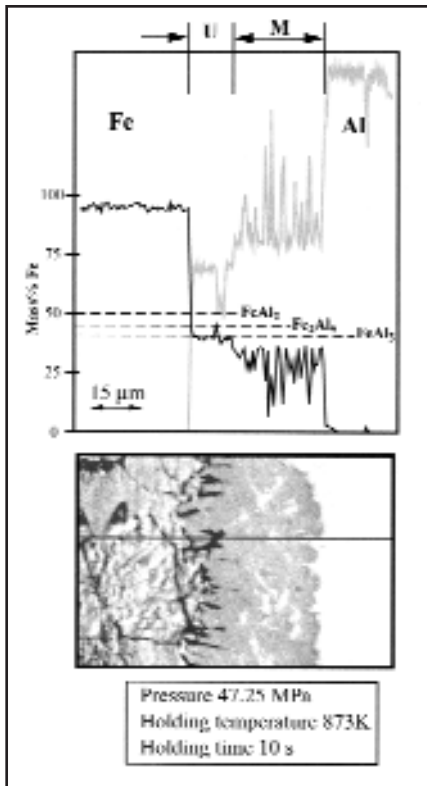


Fig. 5 — EPMA traces of Fe and Al across the diffusion welded joint showing uniform layer and mixed layer.

creep deformation (Ref. 11). This makes an intimate contact over a large fraction of the interface area. When high pressures are applied, not only deformation of asperities takes place but the aluminum oxide film is also broken, improving the interfacial contact area (Ref. 12). Thus, pressure helps in reducing the effective activation energy E_{eff} , which is increased due to the presence of aluminum oxide film. The values of E_{sol} and k_{sol} will remain constant even under varying pressures, because simple diffusion (without formation of intermetallic compound) is involved.

Effect of Interface Layer on Joint Properties

Interface layer thickness has a significant effect on joint strength: the thinner

the layer, the better the strength. Joints were made between steel and aluminum by deformation welding followed by heat treatment (Ref. 13). High values of fracture toughness, G_{IC} , were noted (6097 N/m), when the diameter of the Al-rich Fe_2Al_5 was less than $4 \mu m$. The main reason for embrittlement of these joints was attributed to the formation of Kirkendall porosity rather than the intermetallic compound layer. In the case of resistance spot welding of mild steel and aluminum Alloy 5052 with aluminum clad steel as an insert, an increase in shear strength was observed from 26 to 56 MPa, when the interface layer thickness was reduced from 1.0 to $0.4 \mu m$ (Ref. 6).

Vacuum roll welded joints of mild steel to aluminum Alloy 5083 showed constant shear strength of 60 MPa when the total reduction of sheets was above 5% (Ref. 14). However, shear strength decreased after postheat treatment, as intermetallic compound layer appeared at the interface.

Solid-Liquid Interaction and Use of High-Energy Beams

When joining temperatures are higher than the melting point of aluminum, the process involves solid steel-liquid aluminum interaction. During this type of interaction, three stages are involved (Ref. 9):

- ∑ Wetting of solid steel by molten aluminum,
- ∑ Dissolution of iron into liquid aluminum,
- ∑ Subsequent diffusion of iron in liquid aluminum.

These stages have a strong effect on the structure and properties of the welded joints. In solid-liquid interaction, formation of intermetallic compounds is considerably faster than in solid-solid interaction because atoms have more kinetic energy in the liquid state than in the solid state. However, spreading of liquid aluminum is necessary for effective dissolution and diffusion of iron atoms in it. It was suggested that satisfactory spreading is possible when a sharp, intensified, fast moving heat source such as an electron beam is used (Ref. 9).

The high energy density of such a source will melt aluminum quickly, but the

molten pool will be restricted to a small size. There will be accelerated diffusion of iron atoms in the molten pool of aluminum. Fast motion of the heat source will control contact time between solid steel and liquid aluminum and provide a fast cooling rate. This will restrict diffusion to a limited depth and a thinner intermetallic compound layer will result, which is favorable for improving joint strength. If dissolution and diffusion of iron into liquid aluminum are intensified in this way, iron content may be increased beyond 45 at-% Fe. Such condition will promote formation of Fe-rich intermetallic compounds at the interface and will result in improved joint strength.

A laser beam provides an excellent tool for achieving control over heat input and in reducing the melt pool size (Ref. 15). An Nd:YAG laser has been used with and without Al-12%Si welding wire for the joining of aluminum and steel sheets in overlap configuration (Refs. 15, 16). Their average tensile strength was 171 MPa, with $3 \mu m$ interface layer thickness. The high tensile strength can be attributed to high silicon content because the presence of silicon restricts formation of brittle Al-rich intermetallic compound (Ref. 17).

Fluxes are generally used in brazing and soldering to remove oxides from the base metal surface by a reduction and/or dissolution reaction, to protect the clean surface from reoxidation, and to modify the surface tension of the molten metal (Ref. 18). These functions are helpful during joining of steel and aluminum. Hence, aluminum brazing flux was used in the present work.

The laser roll welding process, which consists of simultaneous laser heating and pressing with a roll, has been suggested by the authors in previous work (Refs. 19–22) to join steel and aluminum. The effect of roll pressure in laser roll welding was investigated previously (Ref. 19). It was noted that, even with low heat input, increased roll pressure improves the contact area and helps in intermetallic compound layer formation. The effect is similar to that found in diffusion welding in which pressure is an important parameter. When diffusion temperature was constant and pressure was in-

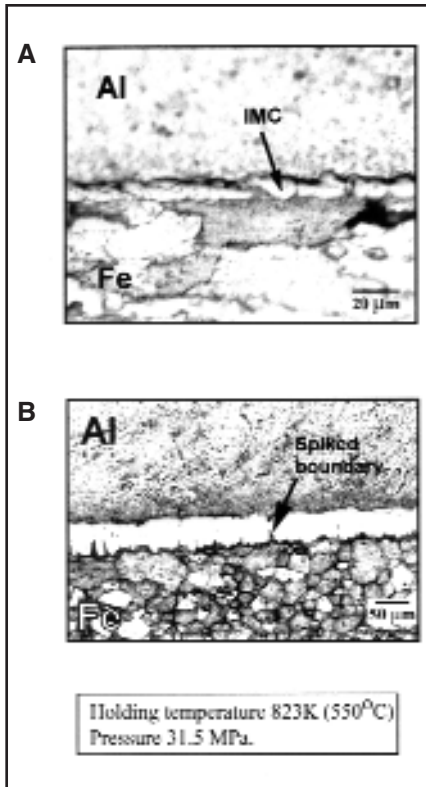


Fig. 6 — Interface microstructures of diffusion welded specimens with different holding times. A — Holding time 100 s; B — holding time 1 h.

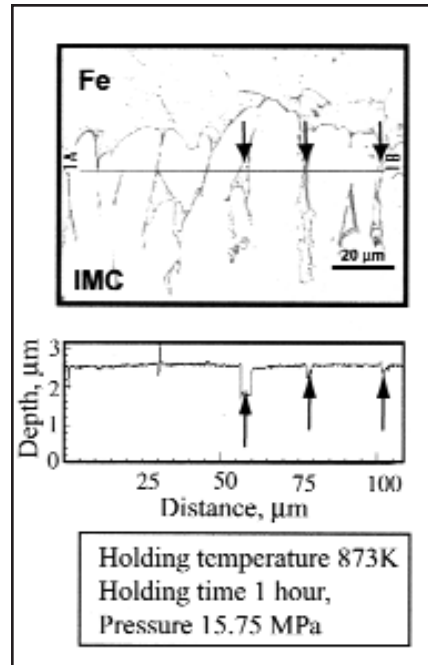


Fig. 7 — Laser beam depth analysis of diffusion welded specimen showing microvoids in interface on steel side. Void locations are shown by arrows.

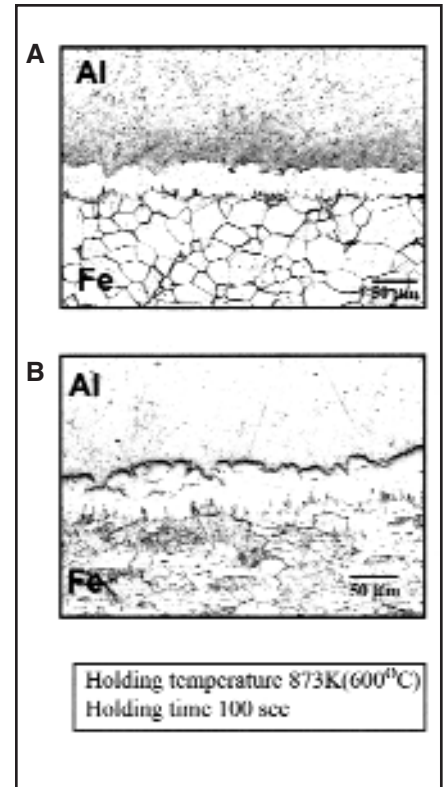


Fig. 8 — Effect of pressure on interface layer microstructure of diffusion welded specimen. A — Pressure 15.75 MPa; B — pressure 47.25 MPa.

creased, incubation time for formation of the interface layer was reduced. With constant diffusion time, an increase in pressure caused formation of the interface layer at lower temperatures. Hence, in both processes, pressure plays an important role in interface layer formation.

With this background, experiments were carried out to join low-carbon steel and aluminum Alloy 5052 by diffusion welding and laser roll welding. Diffusion welding was carried out by varying temperature and time without any insert material. It was decided to understand the effect of pressure on the kinetics of intermetallic compound layer formation during diffusion welding. Activation energy for formation of intermetallic compound (E_{IMC}) and effective activation energy (E_{eff}) values were estimated for different pressures. Time-temperature-phase (TTP) diagrams were plotted for different pressures.

The object of the laser roll welding experiment was to promote formation of slightly ductile Fe-rich intermetallic compounds in the interface layer and thereby improve the joint strength by varying laser heat input and roll pressure. Aluminum brazing flux was applied on the faying surface of the aluminum sheet.

Experimental Procedure

Materials Used

Cold rolled, low-carbon steel sheet with 0.12 wt-% carbon and aluminum Alloy 5052-O sheet were used for joining. For diffusion welding, the thickness of both sheets was 1 mm, whereas for the laser roll welding experiment, 0.5-mm-thick steel sheet and 1-mm-thick aluminum alloy sheet were used.

Diffusion Welding

From Fig. 2, it can be noted that above 723 K (450°C), the diffusion of iron in aluminum is considerably fast. Liquidus and solidus temperatures of 5052 aluminum alloy are 922 K (649°C) and 880 K (607°C), respectively. Therefore, diffusion welding was performed with each permutation of temperature, time, and pressure in the matrix of 773, 798, 823, 848, and 873 K; 2, 10, 100, 500, 1000, and 3600 s; and 15.75, 31.5, and 47.25 MPa.

Generally, diffusion welding is performed by placing sheets of specimen between two punches in a die and the whole assembly is heated externally. This is done to keep pressure constant throughout the

thermal cycle. When diffusion welding of steel-aluminum is made in this way, formation of a brittle intermetallic compound layer at the interface makes the weld too fragile for handling and further characterization becomes difficult. Therefore, to ensure that specimens do not break during characterization, diffusion welding was conducted in such a way that the sheets are not detached from each other in all stages of welding as well as characterization. This was achieved by clamping the sheets with washers, a nut, and a bolt (Material AISI-304). Pressure was applied with a torque meter prior to diffusion welding and was calculated by using a formula for threading-friction between nut and bolt (Ref. 23).

Generally, this method suffers from pressure variation during heating due to thermal expansion. However, pressure remains almost constant during diffusion welding of steel and aluminum, provided the ratio of their thickness is matched with that of their linear coefficients of thermal expansion (α). The values of α for low-carbon steel, 5052 aluminum alloy, and SAE 304 stainless steel are 12.0×10^{-6} , 23.8×10^{-6} , and $18.0 \times 10^{-6} \text{K}^{-1}$, respectively. Thickness of the steel and aluminum sheets are 1 mm each, and they cover a bolt

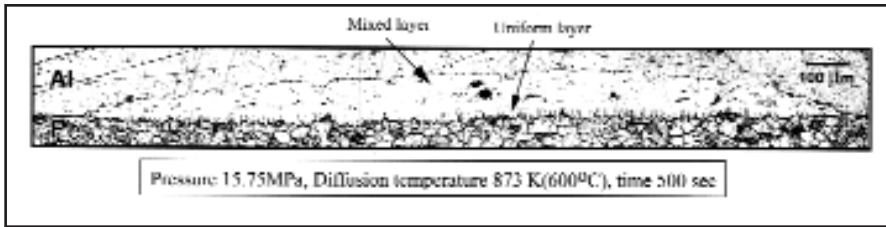


Fig. 9 — Microstructure of diffusion welded low-carbon steel-A5052 alloy joint.

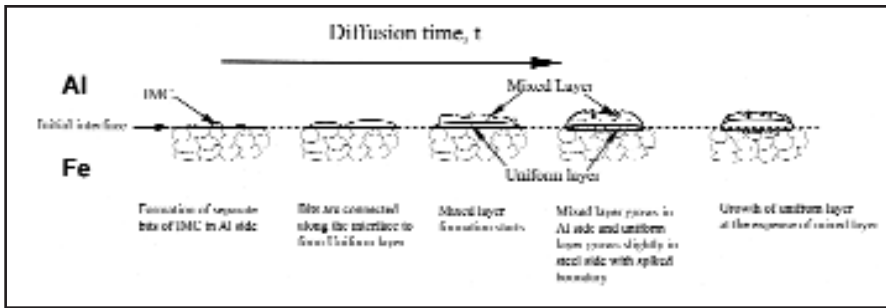


Fig. 10 — Stages in formation of interface layer during diffusion welding of low-carbon steel-A5052 alloy sheets

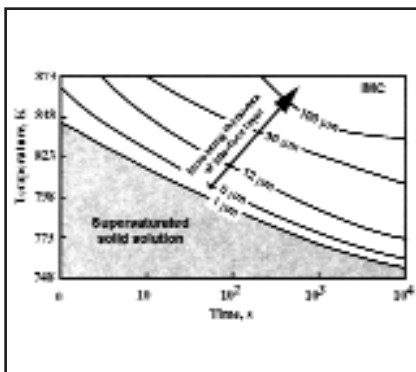


Fig. 11 — Time-temperature-phase (TTP) diagram for diffusion welding of low-carbon steel-5052 Al alloy with a pressure of 31.5 MPa.

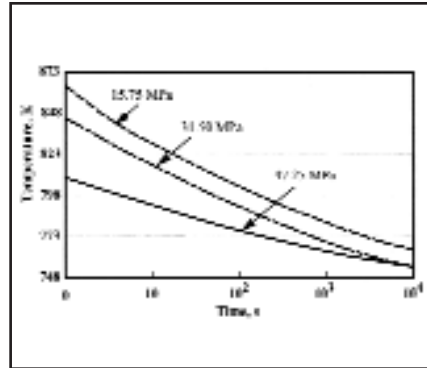


Fig. 12 — Effect of pressure during diffusion welding on the start curves for interface layer formation.

length of 2 mm. Therefore, the change in the length of the bolt is compensated for by the change in thickness of the sheets, i.e., $DL_{Bolt} \oplus (DL_{Steel} + DL_{Al})$ due to heating. For applied pressures of 15.75, 31.5, and 47.25 MPa at room temperature, estimation reveals they will reduce by 0.02–0.07% in the diffusion temperature range of 773–873 K (500–600°C). This variation is negligible and therefore can be ignored.

Sheets of steel and aluminum alloy were cut to square coupons of 30 mm per side with an 8-mm-diameter center hole. Faying surfaces were polished with 200 grit size emery paper followed by ultrasonic cleaning in acetone for 5 min. The steel and aluminum coupons were clamped and pressure was applied with a torque meter. A muffle furnace was

heated to a predetermined diffusion temperature and soaked for 15 min for temperature equalization inside the chamber. The thermal cycle for diffusion welding consisted of three stages: heating, diffusion, and cooling without any protective atmosphere. The heating stage was started by charging a specimen in the furnace. Heating rate was controlled so that diffusion temperature was reached within 20 to 30 s after charging. This was followed by the diffusion stage, which consisted of holding the specimen for a predetermined time at the diffusion temperature. After diffusion, the specimen was quenched in water.

Diffusion welded specimens were mounted in self-setting epoxy resin in the as-clamped condition. The mounted spec-

imens were cut along the bolt axis at the center, ensuring support to the welded sheets while revealing a cross section of the joint on either side of the bolt. The specimens were polished and etched in 3% nital for microstructure observation. Maximum thickness of the interface layer formed was measured for each specimen. Corresponding to the compressive pressures applied, separate TTP diagrams were plotted with diffusion temperature as ordinate and diffusion time as abscissa. The points where intermetallic compound layer thickness was just above 0 μm were joined with a line to show the “start” curve representing incubation times for intermetallic compound formation.

The laser microscopy technique was used for depth analysis to detect pore formation in and around the interface layer. To identify intermetallic compounds present in the layer, EPMA by wavelength dispersive X-ray spectroscopy (WDS) was carried out on the nital-etched specimen. Microhardness was measured across the interface at a 50-g load.

Laser Roll Welding

A schematic diagram of the laser roll welding process is shown in Fig. 3A. A 2.4-kW, continuous-wave CO₂ laser facility was assembled with a flat bending mirror and roll fixture. The roll is made from AISI 304 stainless steel and mounted with a calibrated compression spring for applying predetermined roll pressure. Roll pressure was varied between 150 and 202 MPa. A quasi-Gaussian laser beam (TEM 01* mode) passes through a focusing lens of ZnSe. A flat mirror placed at 57.5 deg with the horizontal reflects the laser beam so that the distance between roll axis and center of the beam spot is reduced to 17 mm. Shape of the beam was a quasi-elliptical spot of 2.5 mm minor diameter across and 3.5 mm major diameter along the direction of table travel. A defocusing distance of –25 mm was used. Details of the clamping sheets on the table are shown in Fig. 3B. The steel sheet is clamped on top of the aluminum alloy sheet with an overlapping width of 3 mm and a gap of 0.2 mm.

Suitable range of laser power and travel speed for laser roll welding was determined by measuring the maximum temperature at the interface. The temperature was also calculated by using the Ashby-Easterling model with conductive mode of heat transfer (Refs. 24, 25).

The thickness of the steel sheet was 0.5 mm and that of the 5052 aluminum alloy was 1.0 mm. Sheets were cut in rectangular pieces with 150 mm length and 45 mm width. After polishing of faying surfaces with a wire brush, both sheets were cleaned in an ultrasonic bath of acetone

for 5 min. The steel surface exposed to the laser beam was coated with graphite to increase absorption of the laser beam. To facilitate fast melting of the aluminum alloy sheet and to remove the oxide film on it, the faying surface was coated with aluminum brazing flux, KAIF_4 : $\text{K}_2\text{AlF}_5 \cdot \text{H}_2\text{O}$ (17–25 wt-%) with particle size of 15 to 21 μm . Argon gas with a 25.0 L/min flow rate was used for shielding. Laser power of 1.5 kW was used for all combinations of travel speeds and roll pressures.

Laser roll welded specimens were cut across the lap joint seam for macrostructure and microstructure observation. Etching with 3% nital was made to reveal the interface layer. The thickness of the interface layer was measured at five equally spaced locations and its average value reported. Electron-probe microanalysis by WDS was used to analyze the interface layer and to identify the intermetallic compounds present. These results showed linear traces of iron and aluminum contents in wt-%. Based on the composition and mechanical properties shown in Tables 1 and 2, thickness of the interface layer was divided into Fe-rich intermetallic compound thickness ($\text{FeAl} + \text{Fe}_3\text{Al}$) and Al-rich intermetallic compound thickness ($\text{FeAl}_3 + \text{Fe}_2\text{Al}_3$). For the tensile shear test, three samples were cut as per the JIS Z 3192–3B specification with 8 mm width across the lap joint. The tensile shear test was carried out on a universal testing machine.

The sheared surfaces of steel sheet were subjected to X-ray diffraction analysis by using Mo-K α radiation to identify intermetallic compounds present on it. Backscattered electron microscopy was used to observe the remaining aluminum area on the sheared steel surface.

Experimental Results and Discussions

Diffusion Welding

Diffusion welding of similar materials goes through the stages of asperity contact, their deformation, formation of interfacial boundary, grain boundary migration, and volume diffusion with pore elimination (Ref. 11). However, when dissimilar metals are to be joined, the absence or presence of intermetallic compounds on their equilibrium diagram should be carefully observed. When such intermetallic compounds exist, then their diffusion welding will go through two additional stages: formation of supersaturated solid solution and its transformation into intermetallic compound (Ref. 10). Such course of intermetallic compound formation takes place when steel and aluminum are diffusion welded.

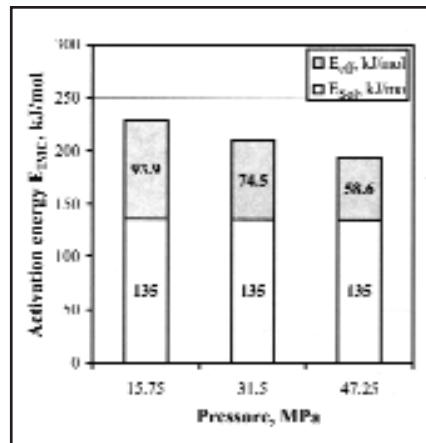


Fig. 13 — Effect of pressure on activation energy for formation of intermetallic compound layer at the interface of diffusion welded low-carbon steel-5052 aluminium alloy joints.

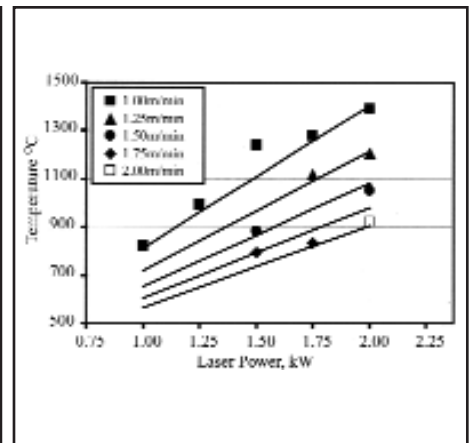


Fig. 14 — Maximum temperatures at the interface when laser heated with different travel speeds and laser powers. Calculated temperatures are shown by lines and measured temperatures are shown by legends.

Microstructure of Interface Layer and Its Development

All intermetallic compound layers appeared white in color after etching with nital. Therefore, the type of intermetallic compounds present cannot be distinguished microscopically.

Figure 4 shows microstructures and respective sketches of diffusion-welded specimens at different temperatures with a diffusion time of 10 s and pressure of 47.25 MPa. Formation of the intermetallic compound layer is shown in Fig. 4A at a diffusion temperature of 823 K (550°C). The intermetallic compound has just started to grow as separate particles (13 μm thickness) at the aluminum side of the interface (i.e., above the initial interface line in Fig. 5A). Such formation in the aluminum side is in agreement with the faster diffusion of iron in aluminum rather than vice versa.

In diffusion welding at 873 K (600°C) (Fig. 4B), the intermetallic compound layer was continuous along the interface and it was thicker (41 μm) than that formed at 823 K (550°C). This layer consists of two distinct parts, a “uniform” layer (U) and a “mixed” layer (M). The uniform layer has a spike-shaped boundary protruding in the steel side and it contains some black lines perpendicular to the interface. As seen in the EPMA traces of Fig. 5, the uniform layer mostly consists of FeAl_3 with 40.7 wt-% Fe. The mixed layer is seen on the aluminum side, and it consists of white islands surrounded by a gray phase. The EPMA trace of aluminum in the mixed layer shows wide variations. The peaks correspond to the white islands of aluminum and the surrounding gray phase is made of the Al-rich intermetallic compound FeAl_3 .

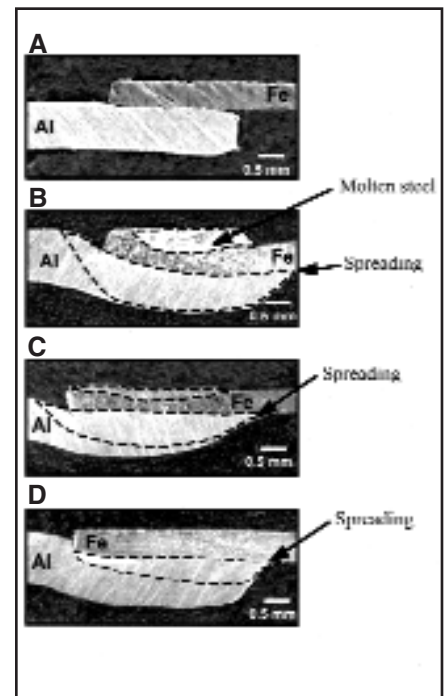


Fig. 15 — Effect of travel speed on macrostructures of laser roll welded specimen. A — Without laser heating; B — 1.5 m/min; C — 1.8 m/min; D — 2.2 m/min.

The effect of holding time on the microstructure of the interface layer is shown in Fig. 6. When holding time was 100 s, temperature 823 K (550°C), and pressure 31.5 MPa (Fig. 6A), the intermetallic compound layer thickness was about 9 μm . With a holding time of 3600 s and the other conditions being the same, the layer thickness increased to 46 μm — Fig. 6B. When holding time was 100 s, particles of intermetallic compound are seen formed and spread partially along the interface. However, they are not yet seen merged

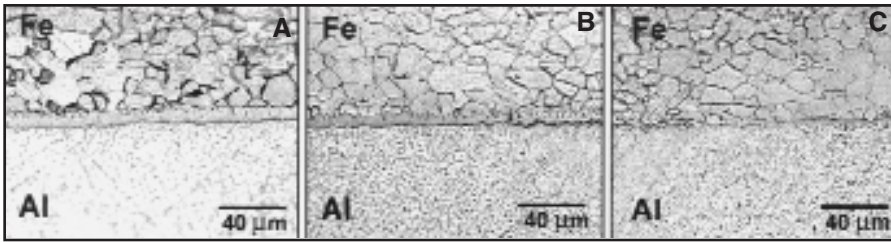


Fig. 16 — Microstructures of laser roll welded specimen showing effect of travel speed. A — 1.8 m/min; B — 2.0 m/min; C — 2.4 m/min.

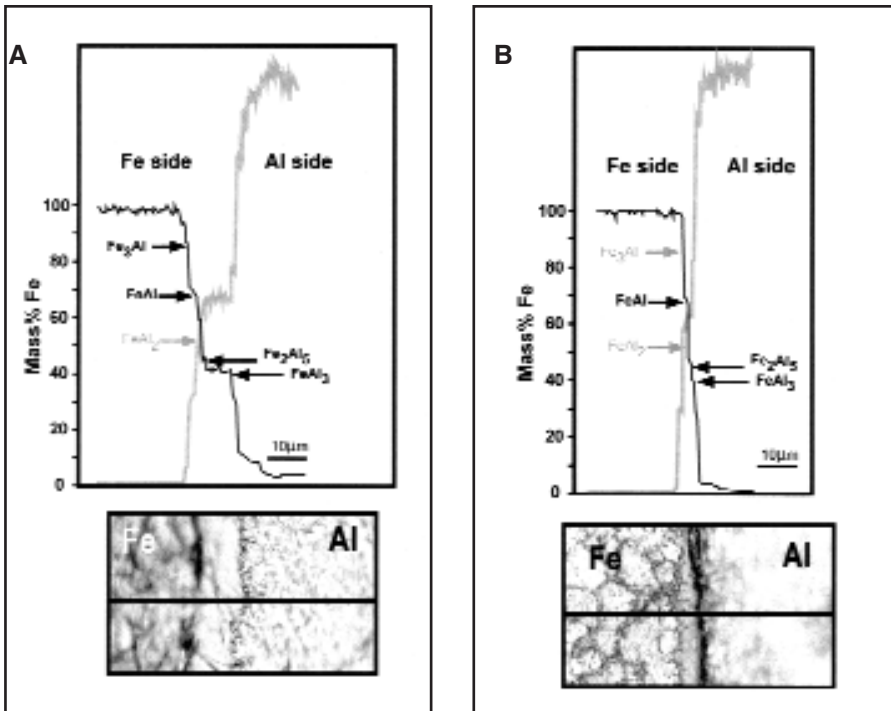


Fig. 17 — Electron-probe microanalysis traces of Fe and Al across laser roll welded interface layer. A — Travel speed 1.2 m/min; B — travel speed 2.0 m/min.

with the neighboring ones — Fig. 6A. In the case of the specimen with a 1-h holding time (Fig. 6B), the interface microstructure shows a uniform layer with spiked boundary on the steel side and the mixed layer is almost absent. The EPMA results show that long diffusion time causes transformation of aluminum islands into FeAl_3 intermetallic compound and, hence, the uniform layer grows at the expense of the mixed layer.

Fine spike lines are seen perpendicular to the interface line in the uniform layer on the steel side (Figs. 4B and 6B). There is considerable migration of iron toward the aluminum side along the grain boundaries and through grains, whereas migration of aluminum is negligible. Therefore, deficiency of iron atoms occurs at some places in the steel side of the interface.

Particularly, migration of iron atoms from grain boundaries and lattice defects is fast as compared to that from the grain bulk. Therefore, deficiency of iron atoms and poor supply of aluminum atoms results in accumulation of microvoids at the grain boundaries and lattice defects. These microvoids grow in size and ultimately form linear voids in the uniform layer. These lines are perpendicular to the interface and indicate strong flow of iron atoms toward the aluminum side. Hence, it is thought that the Kirkendall effect is the reason for linear void formation in the uniform layer.

Depth analysis (on laser microscope) of the diffusion-welded interface has been reported in previous work (Ref. 19). It confirms the existence of voids at the spike lines in the uniform layer — Fig. 7. Mag-

nified microstructure at the steel side of the interface layer is shown on top and corresponding depth values are shown in the bottom graph. Depth values at locations marked with arrows are in the range of 0.7–2.1 μm . These locations correspond to the black lines in the uniform layer. They are deeper than the etched grain boundaries in steel. In the same photograph (Fig. 7), the boundary between steel and intermetallic compound layer is seen as a spiked structure with rounded tips. It is thought that these rounded tips are formed due to diffusion of iron not only from the grain boundaries but also from the bulk grains.

Figure 8 shows the effect of applied pressure on the microstructure of diffusion-welded joints. The conditions were diffusion temperature 873 K (600°C), holding time 100 s, and pressures 15.75 and 47.25 MPa. When pressure was 15.75 MPa, layer thickness measured 37 μm (Fig. 8A), whereas with 47.25 MPa, it measured 59 μm — Fig. 8B. The effect of pressure is also seen on the shape of ferrite grains in steel. Equiaxed grains are seen when pressure is low (15.75 MPa) and elongated grains are seen when pressure increased (47.25 MPa). The uniform layer is thicker and the spiked boundary is coarser in the case of high pressure than that in the case of low pressure. Mixed layers are clearly seen in both microstructures. With high pressure, it is thought that the amount of contact area for diffusion increases and helps in accelerating migration of atoms across the interface.

Figure 9 shows the complete microstructure of the intermetallic compound layer formed along the interface. It was diffusion welded at 873 K (600°C) for 500 s with 15.75 MPa and shows a maximum thickness of about 120 μm . If the thickness is divided into two parts at the original interface line, the thicker part is seen in the aluminum side (about 100 μm) and the thinner one in the steel side (about 20 μm).

From observing the changes in the microstructures with diffusion time, stages in the intermetallic compound layer formation can be understood. They are schematically shown in Fig. 10, as follows:

∑ Formation of separate particles of intermetallic compounds in the aluminum side.

∑ Particles are connected along the interface; start of uniform layer formation.

∑ Mixed layer formation starts in the aluminum side.

∑ The mixed layer grows in the aluminum side and the uniform layer grows slightly in the steel side with spiked boundary.

∑ Growth of the uniform layer at the expense of the mixed layer.

Time-Temperature-Phase Diagram

The TTP diagram for pressure of 31.5 MPa is shown in Fig. 11. The curved lines on the diagram show thickness of the interface layer formed with different combinations of diffusion temperature and time. The line showing 1 μm thickness is the “start” curve for formation of the interface layer. The region below the start curve indicates the “incubation time” during which diffusion continues to form supersaturated solid solution.

The effect of a change in pressure on start curves is shown in Fig. 12. During the early stages of diffusion welding at high temperatures, increasing pressure causes start curves to shift downward, indicating shorter incubation times and lower temperatures for formation of the interface layer with the same thickness. No incubation time was observed for high temperatures of diffusion, which means diffusion starts during the heating stage itself, indicating rapid atomic movement at high temperatures.

High pressures and high temperatures accelerate intermetallic compound formation. There is the combined effect of increased contact area due to pressure and increased atomic mobility due to high temperature. When pressure is increased, contact area increases due to hastening of the initial stages of diffusion, namely surface deformation and asperity collapse (Ref. 11). In addition to increased surface deformation, an increase in pressure also helps in breaking of the aluminum oxide film (Ref. 12).

However, incubation times are longer in the case of low diffusion temperatures. The effect of high pressure on lowering start curves gradually fades away at low diffusion temperatures. At these temperatures, mobility of atoms is reduced due to insufficient kinetic energy. Though asperity collapse, surface deformation, and breaking of oxide film are taking place due to high pressure, longer incubation times are needed at low diffusion temperatures.

Kinetics for Growth of Intermetallic Compound Layer

The effect of temperature on kinetics of diffusion is well known and can be expressed by the Arrhenius equation (Equation 2). The value of activation energy E_{Sol} for diffusion of iron atoms in aluminum lattice is 135 kJ/mol (Ref. 7). The effect of pressure applied during diffusion welding on the effective activation energy E_{Eff} for the formation of the intermetallic compound is quantitatively investigated. The values of E_{IMC} for different pressures were calculated from growth rate and Arrhenius plots. Slope of the Arrhenius plots is the activation energy for intermetallic

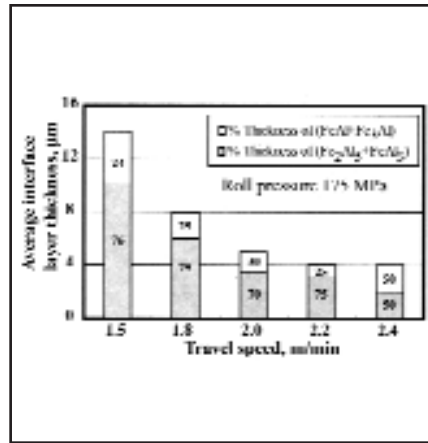


Fig. 18 — Effect of travel speed on average interface layer thickness and percentage of Fe-rich and Al-rich intermetallic compounds.

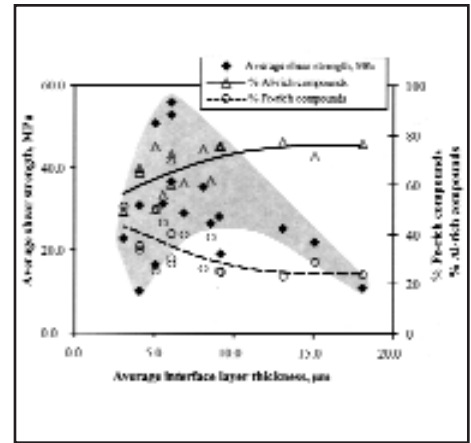


Fig. 19 — Effect of average interface layer thickness on average shear strength of laser roll welded low-carbon steel-5052 aluminium alloy joints.

compound formation.

The maximum value of activation energy for formation of intermetallic compounds E_{IMC} during diffusion welding is 228.9 kJ/mol with an applied pressure of 15.75 MPa. The value of effective activation energy E_{Eff} is given by using Equation 1 (93.9 kJ/mol). As explained in the introduction, E_{Eff} takes into account the factors nW , E_{cr} , and ne (Ref. 10). Factor nW is due to the difference in local composition fluctuations in the aluminum alloy matrix and the intermetallic compound, mostly FeAl₃. A crystal structure change from aluminum to monoclinic FeAl₃ (Table 1) is responsible for increasing the value of E_{cr} . It also causes deformation of matrix increasing ne .

Figure 13 shows the effect of pressure on activation energy for formation of intermetallic compound E_{IMC} . Activation energy decreases from 228.9 to 193.6 kJ/mol as pressure is increased from 15.75 to 47.25 MPa. As explained in the previous section, high pressure increases the metal-to-metal contact area by surface deformation, asperity collapse, and formation of a new surface by breaking the oxide film on the aluminum surface. This decreases effective activation energy E_{Eff} from 93.9 to 58.6 kJ/mol, when pressure is increased from 15.75 to 47.25 MPa. Decrease in effective activation energy E_{Eff} means the energy barrier for diffusion and formation of the intermetallic compound is reduced. In other words, diffusion and intermetallic compound formation are facilitated by increasing pressure.

Temperature Field Simulation for Steel Sheet

Temperature reached at the interface is a critical parameter in laser roll welding of

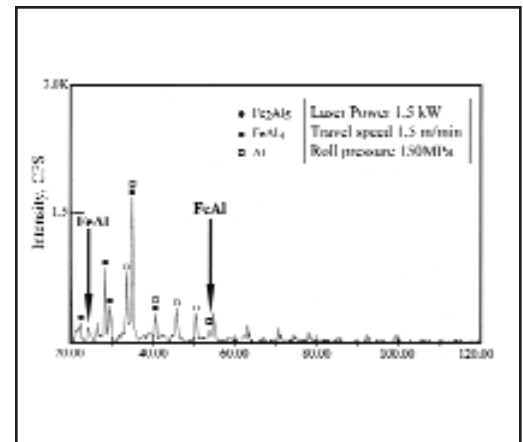


Fig. 20 — X-ray diffraction pattern on steel surface after tensile shear testing. Existence of ductile FeAl intermetallic compound is shown by arrows.

steel to aluminum alloy. For promoting formation of Fe-rich intermetallic compounds in the interface layer, two conditions are important: a large number of iron atoms — beyond 45 at-% Fe — should diffuse in aluminum in a short period of time, and formation of brittle intermetallic compounds should be suppressed.

For accelerated diffusion of iron atoms, liquid aluminum is a better phase than solid and it should wet the steel surface sufficiently (Ref. 9). Therefore, the interface temperature should exceed the liquidus temperature of the aluminum alloy. Because brittle intermetallic compounds are formed between 1433 and 1442 K (1160 and 1169°C), interface temperature should rapidly increase above 1473 K (1200°C). It should also decrease rapidly through that temperature range. Laser heating involves not only a rapid heating rate but also rapid cooling, reducing the time for formation and growth of

brittle intermetallic compounds.

To determine laser power and travel speed suitable to reach this level of temperature at the interface, the Ashby-East-erling model involving laser heating in the conduction mode was used (Refs. 24, 25). In this model, the heat source is considered as a moving finite line situated above the surface and parallel to it. In the present work, the laser beam spot is quasi-elliptical in shape because the incidence angle is 57.5 deg, reducing the energy absorption. Therefore, an absorptivity of 0.3 was used. Other parameters used for calculation of temperature were thermal diffusivity $0.19 \times 10^{-4} \text{ m}^2/\text{s}$, thermal conductivity 15.1 J/m/s/K , and specific heat per volume $9.6 \times 10^6 \text{ J/m}^3/\text{K}$. Calculated and experimentally measured temperatures at the bottom of the steel sheet fairly coincide as shown in Fig. 14. From these results, laser power of 1.5 to 2.0 kW was identified as suitable for laser roll welding. Hence, for laser roll welding, 1.5-kW-laser power was used and travel speed was varied between 1.0 and 3.0 m/min.

Laser Roll Welding

Macrostructures of Laser Roll Welded Joints

The effect of travel speed on macrostructures of laser roll welded specimens with a roll pressure of 202 MPa and laser power of 1.5 kW is shown in Fig. 15. To understand the difference in macrostructures, a photograph of sheets without laser heating is shown in Fig. 15A. When a slow travel speed of 1.5 m/min was used, a considerable change in the original shape is seen — Fig. 15B. The figure shows melting occurs in both the steel and aluminum sheets because of the high amount of laser heat input. Aluminum spreading takes place along the bottom of the steel sheet. Though welding had taken place, it was not uniform. When travel speed is increased to 1.8 m/min, melting of steel in a shallow depth is seen on the top surface. However, the aluminum sheet has undergone considerable melting and spreading — Fig. 15C. With a fast travel speed of 2.2 m/min, the macrostructure shows no melting of steel and aluminum melting and its spreading are limited — Fig. 15D. A similar effect of travel speed on macrostructure was observed with 150 and 175 MPa roll pressures.

Laser heating provides high energy density; therefore, temperature of the steel sheet at the interface rapidly increases above 1473 K (1200°C). When the hot surface of the steel comes in contact with the aluminum due to roll pressure, it melts and spreads along the bottom surface of the steel sheet. Presence of aluminum brazing flux must have supported

in these stages. This situation leads to solid-liquid interaction and accelerates iron diffusion in molten aluminum.

Microstructure and Thickness of Interface Layer

Interface microstructures of laser roll welded joints with 175-MPa roll pressure and 1.5-kW laser power are shown in Fig. 16. In contrast to the microstructures produced by diffusion welding, microstructures of the laser roll welded specimen showed only the “uniform” layer, irrespective of travel speed and roll pressure. The “mixed” layer is completely missing. For a slow travel speed of 1.8 m/min and 175-MPa roll pressure, the average layer thickness is $8 \mu\text{m}$ — Fig. 16A. A spiked boundary at the steel side of the interface layer is seen similar to that observed in diffusion-welded joints. With the slow travel speed, the Kirkendall effect is active in forming microvoids along the spiked boundary; but they are fine due significantly to the short times for diffusion.

For the intermediate travel speeds, the average interface layer thickness is reduced sharply. When travel speed is 2.0 m/min, the interface thickness is $5 \mu\text{m}$ and the spiked boundary is not seen — Fig. 16B. When travel speed is increased further to 2.4 m/min, the interface layer further reduces to $4 \mu\text{m}$ without spiked boundary — Fig. 16C. For all roll pressures used, a similar effect of reduction in interface layer thickness with increasing travel speed was observed.

The backscattered electron image showed a dendritic structure in the heat-affected zone of aluminum adjacent to the interface layer, confirming aluminum melting during laser roll welding.

Effect of Travel Speed on Composition of Interface Layer

As the optical microstructure does not reveal the details of the interface layer, EPMA of iron and aluminum across it were made to identify intermetallic compounds. Two such traces for specimens welded with a pressure of 150 MPa and travel speeds of 1.2 and 2.0 m/min are shown in Fig. 17. Intermetallic compounds in the interface layer are shown in dark bold letters and black arrows. Faint gray letters and arrows are used for those intermetallic compounds not present in the interface layer.

Variation in composition of the intermetallic compound layer is seen as stepped lines. Some intermetallic compounds are very narrow in thickness and are closely spaced together. Therefore, overlapping of electron beam on neighboring intermetallic compounds gives in-

termediate composition, which is inaccurate. Sometimes presence of complex mixed structure may also yield an inaccurate result. When intermetallic compounds are very thin, as seen in Fig. 17B, it is difficult to estimate exact composition.

With a slow travel speed of 1.2 m/min, FeAl_3 is predominantly observed on the aluminum side with some Fe_2Al_5 at the center — Fig. 17A. On the steel side, the layer mainly consists of FeAl with some Fe_3Al . For a faster travel speed of 2.0 m/min, the interface layer has become thinner and the thickness of FeAl_3 is further reduced — Fig. 17B. From Table 2, it can be noted that FeAl_3 and Fe_2Al_5 are hard and brittle, whereas FeAl and Fe_3Al are slightly ductile. Hence, the interface layer is divided into a brittle part ($\text{FeAl}_3 + \text{Fe}_2\text{Al}_5$) and a slightly ductile part ($\text{FeAl} + \text{Fe}_3\text{Al}$), based on the composition given by the EPMA traces. The fraction of these parts is expressed in percentage with respect to total thickness of interface layer.

Figure 18 shows the effect of travel speed on average interface layer thickness and the percentages of the Al-rich ($\text{FeAl}_3 + \text{Fe}_2\text{Al}_5$) and Fe-rich parts ($\text{FeAl} + \text{Fe}_3\text{Al}$) in it, as measured from the EPMA results. Changes taking place with a roll pressure of 175 MPa are shown in Fig. 18. Average interface layer thickness decreases sharply from 14 to $8 \mu\text{m}$ when the travel speed increases from 1.5 to 1.8 m/min; but the percentage thickness of the Al-rich part reduces slightly from 76 to 75%. As the travel speed increases in the intermediate range of 1.8–2.0 m/min, average interface layer thickness decreases slowly from 8 to $5 \mu\text{m}$. In this intermediate range, the thickness of the Al-rich intermetallic compounds decreases from 75 to 70%. For a higher travel speed of 2.4 m/min, total interface layer thickness is reduced further to $4 \mu\text{m}$ and the percentage of Al-rich intermetallic compound decreases to 50%. As the travel speed increases, percentage of Fe-rich intermetallic compound increases at the expense of the Al-rich intermetallic compounds. Similar effect of travel speed on composition of interface layer was seen for roll pressures of 150 and 202 MPa.

Laser heating and the presence of aluminum brazing flux have caused rapid melting and spreading of aluminum above 1473 K (1200°C). Simultaneously, diffusion of a large number of iron atoms in liquid aluminum might have caused formation of Fe-rich intermetallic compound on the steel side of the interface (Ref. 9). The thermal cycle of laser heating provides a condition that is far away from equilibrium, and time for formation of brittle Al-rich intermetallic compounds on the steel side is not sufficient. Therefore, formation

of brittle Al-rich intermetallic compounds is suppressed and that of the Fe-rich intermetallic compounds is promoted, at least on the steel side of the interface layer. Electron-probe microanalysis results showed that complete elimination of Al-rich brittle intermetallic compounds is not taking place. They are always formed on the aluminum side of the interface layer. This may be attributed to the presence of the large amount of aluminum and to their low free energy values (Ref. 4).

Tensile Shear Test Results

When a lap joint of dissimilar metals is subjected to tensile shear testing, the specimen may fail either at the interface or in the weaker base metal. When failure occurs at the interface, the shear strength of the joint is calculated based on the overlap area. If the specimen fails in the weaker base metal, it always fails in the tensile mode. Failure of the weaker base metal in tension indicates that the shear strength of the joint is greater than the tensile strength of the weaker base metal. When the weaker base metal fails, joining of the dissimilar metals can be regarded as successful. However, the exact value of the joint's shear strength remains unknown.

The tensile shear test specimen has a width of 8.0 mm. Tensile strength of the 5052-O aluminum alloy is 200 MPa and its cross-sectional area 8.0 mm² (with a thickness of 1.0 mm), hence it will support a maximum tensile force of 1.6 kN. The tensile strength of low-carbon steel is 300 MPa and its cross-sectional area is 4.0 mm² (with a thickness of 0.5 mm); hence, it will support a maximum tensile force of 1.2 kN. Therefore, the steel side of the joint will fail first due to its smaller cross section (even though it has a higher tensile strength), whereas the cross section of the aluminum alloy is twice that of the steel and will therefore have a greater load-carrying capacity (despite its lower yield strength). The steel side will fail if the joint has a higher shear strength than 50 MPa as shear area is 24 mm² (8 mm wide \times 3 mm overlap length).

With slow travel speeds, there is excessive laser heat input and the cooling rate is slow. This provides sufficient time for diffusion and formation of a thick interface layer containing a large amount of Al-rich brittle intermetallic compounds. Such an interface structure drastically reduces the joint strength. When travel speeds are fast, there is insufficient heat and time for melting of the aluminum and the diffusion process to take place. This results in incomplete welding at the interface and poor shear strength. Intermediate travel speeds provide an adequate amount of heat and cooling rate, so that a thin con-

tinuous interface layer is formed with a reduced amount of brittle Al-rich intermetallic compound — Fig. 18.

When the average interface layer thickness is between 4 and 5 μm with the percentage of Fe-rich intermetallic compounds between 25 and 40%, shear strength reaches a maximum value between 50.8 and 55.9 MPa — Fig. 19. These specimens failed partially — at the interface and in aluminum. The rest of the specimens — belonging to all combinations of roll pressure and travel speed — failed at the interface. This indicates that the joints have a lower shear strength than the tensile strength of the low-carbon steel sheet, which has a lower load-carrying capacity in the present combination. The reason for this may be attributed to the large amount of Al-rich brittle intermetallic compounds (60–75%) still present in the interface layer. However, promotion of Fe-rich intermetallic compounds in the layer has improved the shear strength from 11.0 to 55.9 MPa, which is shown as a gray area in Fig. 19. As the intermetallic compound thickness decreases, the amount of Fe-rich intermetallic compounds in it increases and that of Al-rich intermetallic compound decreases — Figs. 18, 19.

X-ray diffraction pattern on steel surface after shear testing is shown in Fig. 20. It shows that the Fe-rich intermetallic compound FeAl exists in the interface layer in addition to Al-rich intermetallic compounds FeAl₃ and Fe₂Al₃. This confirms the promotion of Fe-rich intermetallic compound formation in the interface layer by laser roll welding. A backscattered electron image of the sheared steel surface — belonging to the condition 150 MPa roll pressure and 1.6 m/min travel speed — showed that about 70% area is covered with aluminum.

Conclusions

The present study is focused on joining a dissimilar metal combination of low-carbon steel and 5052 aluminum alloy. Diffusion welding was studied for the effect of pressure on kinetics of interface layer formation. Laser roll welding was investigated to achieve a thin interface layer thickness and to promote a slightly ductile Fe-rich intermetallic compound in it to increase the joint strength. The following conclusions can be drawn.

1) The diffusion welded interface layer contains only the brittle intermetallic compounds FeAl₃ and Fe₂Al₃. It can be divided into two parts: a uniform layer on the steel side and a mixed layer on the aluminum side. The uniform layer consists of FeAl₃ compound and protrudes in the steel side as a spiked boundary. It also con-

tains fine linear voids, which are thought to be the result of the Kirkendall effect. The mixed layer on the aluminum side consists of a mixture of FeAl₃ compound and aluminum.

2) Activation energy for formation of intermetallic compound (E_{IMC}) is greater than that of diffusion of atoms in metals (E_{Sol}). During diffusion welding of low-carbon steel/5052 aluminum alloy, as pressure is increased from 15.75 to 47.25 MPa, the value of E_{Sol} does not change (135 kJ/mol), whereas that of E_{IMC} decreases from 228.9 to 193.6 kJ/mol (with corresponding decrease in E_{Eff}). This indicates that intermetallic compound formation is facilitated by increasing pressure.

3) Laser roll welded joints showed melting and spreading of the aluminum alloy on the bottom surface of the steel sheet. This may be attributed to the high energy density of the laser beam and the presence of flux at the interface. Such melting and spreading might have led to liquid aluminum-solid iron interaction at the interface, accelerating diffusion of iron in liquid aluminum, and promoting slightly ductile Fe-rich intermetallic compound formation. Electron-probe microanalysis results and X-ray diffraction analysis confirmed the existence of Fe-rich intermetallic compounds on the steel side.

4) The effect of roll pressure in laser roll welding was similar to that observed in diffusion welding. It increased the contact area and effectively facilitated diffusion in a short time. Increase in travel speed led to thinning of the interface layer due to reduced laser heat input. Thinning down of the interface layer is also accompanied by an increase in the percentage of Fe-rich intermetallic compounds (FeAl+Fe₃Al) at the expense of Al-rich intermetallic compounds (FeAl₃+Fe₂Al₃). However, complete elimination of brittle intermetallic compounds is not possible due to the large amount of aluminum on the aluminum side of the interface.

5) In the diffusion welded interface layer, Fe-rich compounds were not seen. Laser roll welding achieved their promotion from as low as 23% to as high as 51%. This change in composition of the interface layer improved the shear strength of joints from 11.0 to 55.9 MPa. When the average interface layer thickness is between 4 and 5 μm , with the percentage of Fe-rich intermetallic compounds between 25 and 40%, maximum shear strength is reached between 50.8 and 55.9 MPa.

6) Except for the specimens with shear strength higher than 50 MPa, all laser roll-welded specimens failed at the interface. Therefore, the shear strength of the joints is lower than the tensile strength of the low-carbon steel sheet, which has a lower load-carrying capacity in the present com-

bination. This may be attributed to the large amount of Al-rich brittle intermetallic compounds (60–75%) still present in the interface layer.

Acknowledgment

The authors are thankful to Applied Laser Engineering Center (ALEC), Japan, for its financial help with this research.

References

1. Haraga, K. 2000. Strength properties of aluminium/aluminium and aluminium/steel joints for light weighing of automotive body. *Welding in the World* 44(4): 23–27.
2. Cole, G. S., and Sherman, A. M. 1995. Lightweight materials for automotive applications. *Materials Characterization*, Vol. 35, pp. 3–9.
3. Kattner, U. R., and Burton, B. P. 1993. *Phase Diagrams of Binary Iron Alloys*. Edited by H. Okamoto. Materials Park, Ohio: ASM International, pp.12–28.
4. Robinson, P. M., and Bever, M. B. 1967. Thermodynamic properties. *Intermetallic Compounds*. Edited by J. H. Westbrook. New York, N.Y.: J. Wiley & Sons, p. 69.
5. Das, S. K. 1994. Al-rich intermetallics in aluminium Alloys. *Intermetallic Compounds: Vol. II Practice*. Eds. J. H. Westbrook and R. L. Fleischer. New York, N.Y.: John Wiley & Sons Ltd, pp. 175–198.
6. Yasuyama, M., Ogawa, K., and Taka, T. 1996. Spot welding of aluminium and steel sheet with insert of aluminium clad steel sheet — Part I. *Quarterly Journal of Japan Welding Society* 14(2): 314–320 (in Japanese).
7. Japan Metals Society. 1986. *Metals Data Book*, p. 24–25, Tokyo: Maruzen (in Japanese).
8. Iwamoto, N., Yoshida, M., Tabata, S., Takeuchi, T., and Makino, M. 1975. Diffusion welding of mild steel to aluminium. *Transactions of Japan Welding Research Institute* 4(2): 67–70.
9. Ryabov, V. R. 2001. Welding dissimilar metals: Aluminium alloys to steel. *Proc. IIW Int. Conf. Joining Tech. of Dissimilar Materials and Structural Integrity Problems of So Joined Structures*. Eds. J. Kramer, I. Limpel, P. Stular, and J. Tusek, pp. 127–132. Ljubljana, Slovenia.
10. Larikov, L. N. 1994. Diffusion. *Intermetallic Compounds: Vol. I, Principles*. Eds. J. H. Westbrook and R. L. Fleischer. New York, N.Y.: John Wiley & Sons Ltd, pp. 757–770.
11. *Welding Handbook*, Vol. 2, 8th ed., 1991. Diffusion welding and brazing. Eds. M. M. Schwartz and J. M. Gerken. Miami, Fla.: American Welding Society, pp. 814–837.
12. Elliott, S., and Wallach, E. R. 1981. Joining of aluminium to steel, Part 1 — Diffusion bonding. *Metal Construction* (3): 167–171.
13. Albright, C. E. 1981. The fracture toughness of steel-aluminum deformation welds. *Welding Journal* 60(11): 207-s to 214-s.
14. Mukae, S., Nishio, K., Katoh, M., Inoue, T., and Hatanaka, N. 1991. Development of vacuum roll bonding apparatus and production of clad metals — Part I. *Quarterly Journal of Japan Welding Society* 9(1): 17–23 (in Japanese).
15. Wagner, F., Zerner, I., Kreimeyer, M., Seefeld, T., and Sepold, G. 2001. Characterization and properties of dissimilar metal combinations of Fe/aluminum and Ti/aluminum-sheet materials. *Proc. ICALEO 2001* (CD-ROM).
16. Sepold, G., Schubert, E., and Zerner, I. 1999. Laser beam joining of dissimilar materials. *IIW IV*(734): 1–10.
17. Kurakin, A. K. 1970. Mechanism of the influence of silicon on the processes of the reaction diffusion of iron in aluminum. *Fiz. metal. Metalloved*, no. 1, 105–110.
18. Brandi, S. D., Liu, S., and Indacochea, J. E. 1993. Brazability and solderability of engineering materials. *ASM Handbook*, Vol 6, Welding, Brazing and Soldering, pp. 621–622. Materials Park, Ohio: ASM International.
19. Rathod, M. J., and Kutsuna, M. 2003. Laser roll bonding of A5052 aluminum alloy and SPCC steel. *Quarterly Journal of the Japan Welding Society* 21(2): 282–294 (in Japanese).
20. Kutsuna, M., and Rathod, M. J. 2002. Formation of intermetallic compounds in laser roll bonded low carbon steel and aluminum joints. *Proc. of the 143rd Iron and Steel Institute of Japan Annual Meeting*, p. 360 (in Japanese).
21. Kutsuna, M., Rathod, M. J., and Azar, A. 2002. Laser roll bonding of mild steel to aluminum and control of intermetallic compound layer. *Proc. of ICALEO 2002*. Scottsdale, Ariz., p. 609 (CD-ROM).
22. Rathod, M. J., and Kutsuna, M. 2001. Dissimilar metal joining of aluminium and steel by laser roll bonding process. *Proc. Seventh International Welding Symposium*. Kobe, Japan. Japan Welding Society, pp. 875–880.
23. Yamamoto, A. 1995. *Theory and Design of Nut and Bolt Joining*, pp. 30–35. Tokyo, Japan: Yokendo Publishers (in Japanese).
24. Ashby, M. F., and Easterling, K. E. 1984. The transformation hardening of steel surfaces by laser beams—I. Hypoeutectoid steels. *Acta Metallurgica* 32(11): 1935–1948.
25. Steen, W. M. 1991. *Laser Material Processing*, p. 157. New York, N.Y.: Springer-Verlag.

Preparation of Manuscripts for Submission to the *Welding Journal* Research Supplement

All authors should address themselves to the following questions when writing papers for submission to the *Welding Research Supplement*:

- ◆ Why was the work done?
- ◆ What was done?
- ◆ What was found?
- ◆ What is the significance of your results?
- ◆ What are your most important conclusions?

With those questions in mind, most authors can logically organize their material along the following lines, using suitable headings and subheadings to divide the paper.

- 1) **Abstract.** A concise summary of the major elements of the presentation, not exceeding 200 words, to help the reader decide if the information is for him or her.
- 2) **Introduction.** A short statement giving relevant

background, purpose, and scope to help orient the reader. Do not duplicate the abstract.

3) **Experimental Procedure, Materials, Equipment.**

4) **Results, Discussion.** The facts or data obtained and their evaluation.

5) **Conclusion.** An evaluation and interpretation of your results. Most often, this is what the readers remember.

6) **Acknowledgment, References and Appendix.**

Keep in mind that proper use of terms, abbreviations, and symbols are important considerations in processing a manuscript for publication. For welding terminology, the *Welding Journal* adheres to AWS A3.0:2001, *Standard Welding Terms and Definitions*.

Papers submitted for consideration in the *Welding Research Supplement* are required to undergo Peer